JCI The Journal of Clinical Investigation

Inhibiting pathologically active ADAM10 rescues synaptic and cognitive decline in Huntington's disease

Elena Vezzoli, Ilaria Caron, Francesca Talpo, Dario Besusso, Paola Conforti, Elisa Battaglia, Elisa Sogne, Andrea Falqui, Lara Petricca, Margherita Verani, Paola Martufi, Andrea Caricasole, Alberto Bresciani, Ottavia Cecchetti, Pia Rivetti di Val Cervo, Giulio Sancini, Olaf Riess, Hoa Nguyen, Lisa Seipold, Paul Saftig, Gerardo Biella, Elena Cattaneo, Chiara Zuccato

Research Article   **Neuroscience**

A disintegrine and metalloproteinase 10 (ADAM10) is implicated in synaptic function through its interaction with postsynaptic receptors and adhesion molecules. Here, we report that levels of active ADAM10 are increased in Huntington's disease (HD) mouse cortices and striata and in human postmortem caudate. We show that, in the presence of polyglutamine-expanded (polyQ-expanded) huntingtin (HTT), ADAM10 accumulates at the postsynaptic densities (PSDs) and causes excessive cleavage of the synaptic protein *N*-cadherin (N-CAD). This aberrant phenotype is also detected in neurons from HD patients where it can be reverted by selective silencing of mutant HTT. Consistently, ex vivo delivery of an ADAM10 synthetic inhibitor reduces N-CAD proteolysis and corrects electrophysiological alterations in striatal medium-sized spiny neurons (MSNs) of 2 HD mouse models. Moreover, we show that heterozygous conditional deletion of ADAM10 or delivery of a competitive TAT-Pro-ADAM10$^{709-729}$ peptide in R6/2 mice prevents N-CAD proteolysis and ameliorates cognitive deficits in the mice. Reduction in synapse loss was also found in R6/2 mice conditionally deleted for ADAM10. Taken together, these results point to a detrimental role of hyperactive ADAM10 at the HD synapse and provide preclinical evidence of the therapeutic potential of ADAM10 inhibition in HD.

Find the latest version:

https://jci.me/120616/pdf

Inhibiting pathologically active ADAM10 rescues synaptic and cognitive decline in Huntington's disease

Elena Vezzoli,[1,2] Ilaria Caron,[1,2] Francesca Talpo,[3] Dario Besusso,[1,2] Paola Conforti,[1,2] Elisa Battaglia,[1,2] Elisa Sogne,[4] Andrea Falqui,[4] Lara Petricca,[5] Margherita Verani,[5] Paola Martufi,[5] Andrea Caricasole,[5] Alberto Bresciani,[5] Ottavia Cecchetti,[5] Pia Rivetti di Val Cervo,[1,2] Giulio Sancini,[6] Olaf Riess,[7] Hoa Nguyen,[7] Lisa Seipold,[8] Paul Saftig,[8] Gerardo Biella,[3] Elena Cattaneo,[1,2] and Chiara Zuccato[1,2]

[1]Department of Biosciences, University of Milan, Milan, Italy. [2]Istituto Nazionale di Genetica Molecolare "Romeo ed Enrica Invernizzi," Milan, Italy. [3]Department of Biology and Biotechnologies, University of Pavia, Pavia, Italy. [4]King Abdullah University of Science and Technology (KAUST), Biological and Environmental Science & Engineering (BESE) Division, NABLA Lab, Thuwal, Saudi Arabia. [5]IRBM Science Park SpA, Pomezia, Italy. [6]School of Medicine and Surgery, Nanomedicine Center, Neuroscience Center, University of Milano-Bicocca, Monza, Italy. [7]Institute of Medical Genetics and Applied Genomics, University of Tuebingen, Tuebingen, Germany. [8]Institute of Biochemistry, Christian Albrechts University of Kiel, Kiel, Germany.

A disintegrine and metalloproteinase 10 (ADAM10) is implicated in synaptic function through its interaction with postsynaptic receptors and adhesion molecules. Here, we report that levels of active ADAM10 are increased in Huntington's disease (HD) mouse cortices and striata and in human postmortem caudate. We show that, in the presence of polyglutamine-expanded (polyQ-expanded) huntingtin (HTT), ADAM10 accumulates at the postsynaptic densities (PSDs) and causes excessive cleavage of the synaptic protein N-cadherin (N-CAD). This aberrant phenotype is also detected in neurons from HD patients where it can be reverted by selective silencing of mutant HTT. Consistently, ex vivo delivery of an ADAM10 synthetic inhibitor reduces N-CAD proteolysis and corrects electrophysiological alterations in striatal medium-sized spiny neurons (MSNs) of 2 HD mouse models. Moreover, we show that heterozygous conditional deletion of ADAM10 or delivery of a competitive TAT-Pro-ADAM10[709–729] peptide in R6/2 mice prevents N-CAD proteolysis and ameliorates cognitive deficits in the mice. Reduction in synapse loss was also found in R6/2 mice conditionally deleted for ADAM10. Taken together, these results point to a detrimental role of hyperactive ADAM10 at the HD synapse and provide preclinical evidence of the therapeutic potential of ADAM10 inhibition in HD.

Introduction

Huntington's disease (HD) is an autosomal dominant neurodegenerative disorder caused by a polyglutamine (polyQ) expansion in the huntingtin (HTT) protein (1, 2). HTT is localized at the synapse, where it binds to proteins involved in neurotransmitter transport, as well as pre- and postsynaptic organization and function, suggesting that it acts as an important regulator of synaptic activity (3, 4). In contrast, mutant HTT impairs synaptic function in HD (5, 6). This defect occurs early in the disease, in the absence of manifested neuron loss, and is most likely the source of emotional, cognitive, learning, and memory symptoms in HD patients (7). A key factor in this decline is the progressive loss of excitatory corticostriatal glutamatergic input to medium-sized spiny neurons (MSNs), which has been linked to cell-autonomous and neuronal network mechanisms (5, 6).

A disintegrine and metalloproteinase 10 (ADAM10), a member of the large ADAM transmembrane protein family, is expressed at high levels in the brain and regulates the molecular organization and activity of the excitatory synapse by shedding postsynaptic proteins,

including N-cadherin (N-CAD), amyloid precursor protein, nectin-1, prion protein, neuroligin-1, neural cell adhesion molecule L1, and ephrin A2 and A5 (8, 9). ADAM10-mediated shedding of cell-adhesion molecules at the synapse activates a number of processes critical to proper formation, maintenance, and function of the excitatory synaptic circuitries (9). Dendritic spine development, synapse plasticity, memory, and learning all rely on ADAM10 activity (9, 10). The importance of ADAM10 for the homeostasis of adult neuronal networks has been underscored by the observation that the conditional homozygous inactivation of the ADAM10 gene in the neural lineage determines profound synaptic phenotypes in the mouse brain (10, 11). In addition, the overexpression of the enzyme causes unbalance in the expression of genes involved in synaptic transmission, and moderate neuronal damage (12, 13). Consequently, impairments in ADAM10 level and/or activity are detrimental for the human brain. ADAM10 has been linked to epilepsy, Alzheimer's disease (AD), and the developmental disorder Fragile X syndrome (9).

Considering the crucial role of ADAM10 in excitatory synaptic function and based on previous findings that normal HTT regulates its activity in the adult mammalian brain (14), we assessed whether the presence of a pathological polyQ tract in HTT could affect the level of the active form of ADAM10 in the HD brain, with consequences for the function of the excitatory synapse and cognition in HD. In this study, we show that the hyperactivity of ADAM10 and the increased proteolysis of its synaptic substrate N-CAD are decisive neurotoxic events in HD synaptic and cognitive decline.
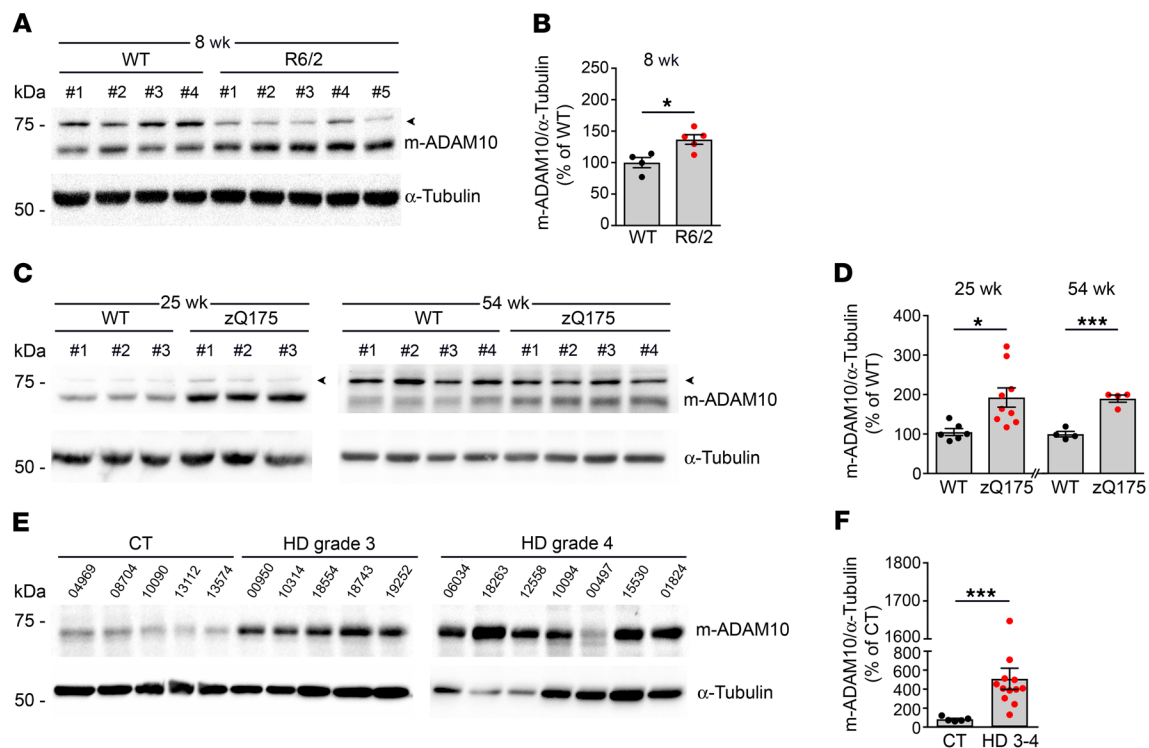
Figure 1. The mature active form of ADAM10 is increased in HD mouse and human striatum. (**A**) Representative Western blot for m-ADAM10 in the striata of WT (*n* = 4) and R6/2 mice (*n* = 5) at 8 weeks of age. (**B**) Quantification of data shown in **A**. *$P < 0.05$, unpaired *t* test. (**C**) Representative Western blot for m-ADAM10 in the striata of WT and heterozygous zQ175 mice at 25 and 54 weeks of age. (**D**) Quantification of data shown in **C**. 25 weeks: *n* = 6-9 mice/genotype; 54 weeks: *n* = 4 mice/genotype. *$P < 0.05$; ***$P < 0.001$, unpaired *t* test. (**E**) Representative Western blot of m-ADAM10 in the postmortem caudate of control (*n* = 5) and HD patients with Vonsattel grades 3 and 4 of neostriatal atrophy (*n* = 12). (**F**) Quantification of data shown in **E**. ***$P < 0.001$, nonparametric Mann-Whitney 2-tailed *U* test. α-Tubulin, loading control. Data are represented as mean ± SEM. Arrowheads, nonspecific bands.

Results

The mature active form of ADAM10 is increased in HD mouse and human striatum. Nascent ADAM10 is produced as an approximately 95 kDa zymogen and matures into a 60 kDa active protease (m-ADAM10) after cleavage of its prodomain, which keeps the enzyme in an inactive state, by furin or proconvertase 7 (PC7), in the trans-Golgi secretory pathway (9). Initially, we evaluated m-ADAM10 levels in R6/2 transgenic mice, which bear a genomic fragment containing the promoter and exon 1 of human *HTT* with 144 CAGs (15). These mice present with early onset and fast disease progression: subtle symptoms begin at 6 weeks of age and become more prominent at 8 to 10 weeks, until the animals die at 13 to 16 weeks (15). Western blot performed with an antibody able to detect the mature active form of the enzyme (10) revealed a 36.7% increase in m-ADAM10 in the striatum of early symptomatic 8-week-old R6/2 mice compared with controls (Figure 1, A and B). We further investigated m-ADAM10 levels in the striatum of heterozygous zQ175 knockin mice in which mouse *Hdh* exon 1 was replaced with a mutated version of human *HTT* exon 1 (16). These mice show a late-onset phenotype and slowly progressive HD pathology (16). We found an 87.5% increase in the level of m-ADAM10 in early symptomatic mutant mice at 25 weeks of age compared with WT mice, a phenotype that persisted at a later time point (54 weeks; Figure 1, C and D). The observed increase in striatal m-ADAM10 levels in HD animals was not due to increased ADAM10 transcription, as quantitative reverse transcription PCR (qRT-PCR) did not reveal differences in the ADAM10 mRNA levels

between R6/2 and WT mice as HD progressed (Supplemental Figure 1; supplemental material available online with this article; https://doi.org/10.1172/JCI120616DS1). Notably, a 56.3% increase of m-ADAM10 was found in the R6/2 cerebral cortex (Supplemental Figure 2, A and B), but not in the cerebellum, which is less affected in HD (Supplemental Figure 2, C and D) (2). Notably, levels of m-ADAM10 were higher in 12 postmortem caudate specimens from HD human subjects with Vonsattel grades 3–4 neostriatal atrophy compared with 5 controls (Figure 1, E and F, and Table 1). Striatal levels of the catalytically active forms of 2 other members of the ADAM transmembrane protein family, ADAM9 and ADAM17, which are enriched in the CNS, did not vary between WT and R6/2 mice at 8 weeks of age (Supplemental Figure 3, A–D) (9). Similar results were obtained when WT and heterozygous zQ175 mice were analyzed (Supplemental Figure 3, E–H). Finally, m-ADAM10 levels were unaffected in the cerebellum of a mouse model of spinocerebellar ataxia type 3 (SCA3) and in 2 transgenic SCA17 rodent models (Supplemental Figure 4, A–F) (17–19). Taken together, these results indicate that 2 mouse models of HD, but not other polyQ disorders, and human HD brain samples exhibit increased levels of the mature form of ADAM10, which is restricted to brain areas that predominantly degenerate in HD.

m-ADAM10 accumulates at the synapse and causes N-CAD proteolysis in HD. Having established that the presence of mutant HTT leads to increased levels of active ADAM10, we investigated possible mechanisms through which this effect may occur. One possibility is that HTT may influence ADAM10 function by interacting with

Table 1. HD patient demographics

ID sample	Vonsattel grade	Age (yr)	Sex	PMI (h)	Region
04969	Control	60	F	21.67	Caudate
08704	Control	70	M	23.50	Caudate
10090	Control	52	M	13.12	Caudate
13112	Control	63	M	17.92	Caudate
13574	Control	53	M	21.06	Caudate
16413	1	68	F	8.30	Caudate
13777	1	52	F	24.40	Caudate
01517	1	55	M	21.70	Caudate
08302	2	76	M	19.90	Caudate
18185	2	55	F	22.60	Caudate
04466	2	54	M	21.80	Caudate
00950	3	69	M	10.10	Caudate
10314	3	70	M	18.00	Caudate
18554	3	60	M	14.90	Caudate
18743	3	53	M	17.80	Caudate
19252	3	58	F	15.40	Caudate
06034	4	35	M	23.90	Caudate
18263	4	54	F	21.70	Caudate
12558	4	50	F	24.30	Caudate
10094	4	33	M	22.00	Caudate
00497	4	48	F	7.58	Caudate
15530	4	64	F	18.20	Caudate
01824	4	45	M	21.60	Caudate

PMI, Postmortem interval; F, female; M, male. Samples were obtained from the HBTRC.

ADAM10 in a polyQ-sensitive fashion. We therefore ectopically expressed HA-tagged WT or mutant full-length HTT carrying 23 or 83Q, respectively, with ADAM10-3XFLAG in HEK293T cells, followed by immunoprecipitation with an anti-FLAG antibody and immunoblotting with an anti-HA antibody. We found that WT HTT coimmunoprecipitated with the ADAM10 zymogen and its active form while the polyQ-expanded HTT did not (Supplemental Figure 5). We therefore speculated that, under HD conditions, ADAM10 may more promptly localize at the plasma membrane and pathologically affect the activity of its synaptic targets. We prepared PSD-enriched Triton-X insoluble fraction (TIF) from a pool of cortical and striatal samples collected from WT and R6/2 mice at 6 and 12 weeks of age. In accordance with our hypothesis, we observed that synaptic levels of m-ADAM10 were increased by 102.5% and 73.5% respectively in R6/2 mice at 6 and 12 weeks of age compared with WT mice (Figure 2, A and B). Similarly, synaptic fractions prepared from postmortem caudate tissues from individuals with early- and late-stage HD showed an increase in m-ADAM10 compared with healthy controls (Figure 2, C and D). The increased pool of m-ADAM10 at the synapse suggests that processing of its synaptic substrates may be increased in the HD brain. Among the ADAM10 targets, N-CAD plays a central role in the regulation of cell-cell adhesion, synapse morphology, and plasticity (20, 21). An excessive presence of ADAM10-mediated N-CAD proteolysis in the brain, documented by increased levels of the 36 kDa N-CAD C-terminal fragment (CTF), affects synaptic connectivity because it compromises adhesion between the pre- and postsynaptic membrane and reduces the overall long-term stability and neurotransmission of the

excitatory synapse (20–22). Thus, we evaluated N-CAD proteolysis in striatal protein lysates from R6/2 mice at 8, 10, and 12 weeks of age. We found that levels of the 36 kDa CTF were 48.4% higher in the striatum of R6/2 mice at 8 weeks of age compared with those in controls (Figure 2, E and G). Levels of the striatal N-CAD CTF further increased by 111% and 162%, respectively, in R6/2 mice at 10 and 12 weeks of age compared with those in controls (Figure 2, E and G). Similarly, a 120.9% increase in N-CAD CTF levels was found in the cortex of R6/2 mice at 12 weeks of age compared with those in controls (Figure 2, F and G). We concluded that mutant HTT causes an accumulation of active ADAM10 at the PSD, leading to increased N-CAD proteolysis.

Allele-specific downregulation of mutant HTT prevents increased levels of m-ADAM10 and N-CAD proteolysis in human HD neurons. To evaluate the link between mutant HTT and the ADAM10/N-CAD pathway specifically in HD human neurons, we exposed iPS cells from control (Q21n1) and HD (Q109n1) patients to a neuronal differentiation protocol (23). A 130% increase in the levels of m-ADAM10 and a 97% increase in N-CAD CTF levels were observed in DIV30 neurons derived from Q109n1 compared with Q21n1 (Figure 3, A–D), reproducing what we previously observed in the brains of HD mice and in the human postmortem caudate tissue. We also tested whether downregulation of mutant HTT might reduce or reverse its adverse effect on the ADAM10/N-CAD pathway. We used an allele-specific zinc finger protein repressor type A (ZFP-A) under the control of the human synapsin-1 (*SYN1*) promoter, which allows a specific targeting of the mutant *HTT* allele in neurons. As expected, ZFP-A expression upon 10 days of infec-
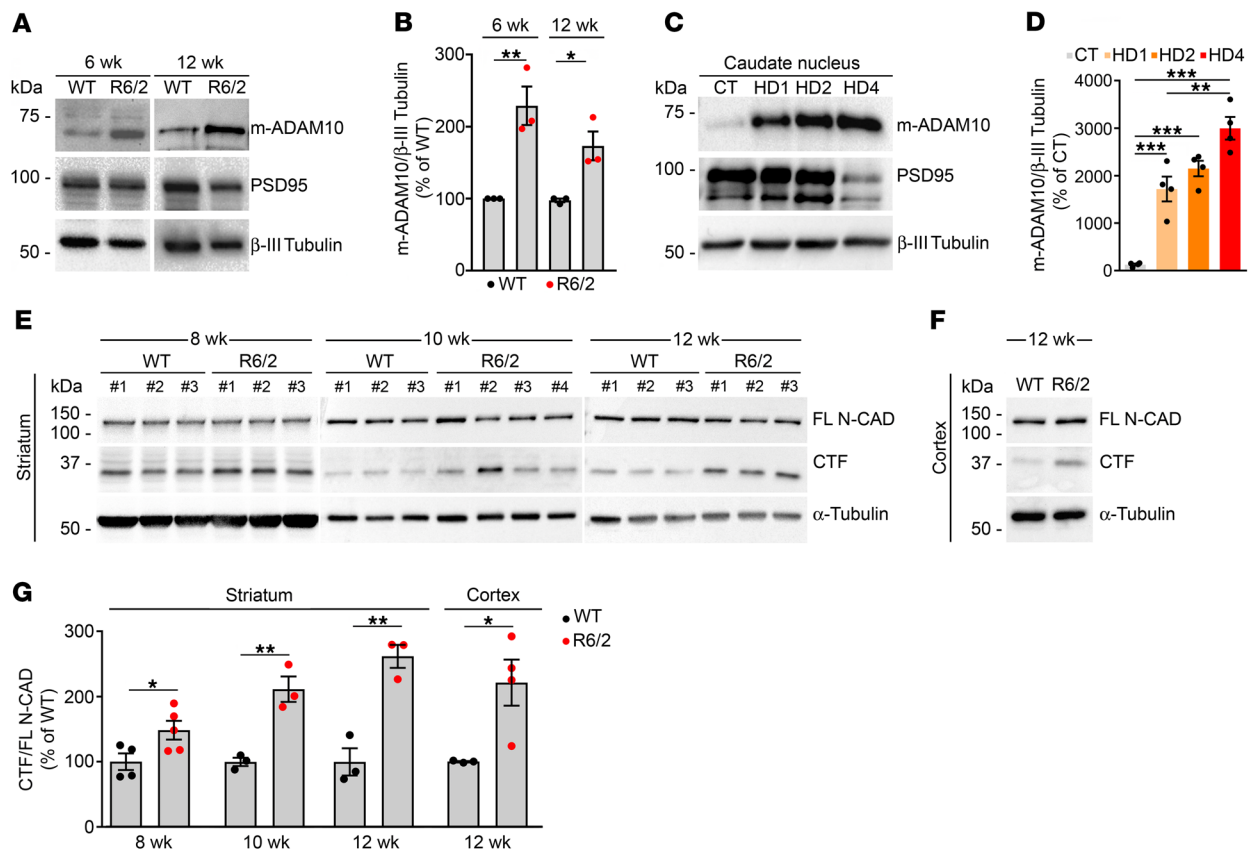
Figure 2. m-ADAM10 accumulates at the synapse and causes N-CAD proteolysis in the HD brain. (**A**) Representative Western blot for m-ADAM10 on PSDs from a pool of n = 3 cortices and striata of WT and R6/2 mice at 6 and 12 weeks of age. β-III Tubulin, loading control; PSD95, PSDs marker. (**B**) Quantification of data in **A**. Data are represented as mean ± SEM of n = 3 biological replicates in which a pool of n = 3 mice/genotype was tested. *P < 0.05; **P < 0.01, unpaired t test. (**C**) Representative Western blot for m-ADAM10 on PSDs prepared from a pool of n = 3 postmortem caudate tissues of control and HD patients with Vonsattel grades 1, 2, and 4 of neostriatal atrophy. (**D**) Quantification of data in **C**. Data are represented as mean ± SEM of n = 4 technical replicates. **P < 0.01; ***P < 0.001, 1-way ANOVA with Bonferroni's post hoc test. (**E**) Representative Western blot of N-CAD CTF in striata from WT and R6/2 mice at 8, 10. and 12 weeks of age. α-Tubulin, loading control. (**F**) Representative Western blot of N-CAD CTF in cortices from WT and R6/2 mice at 12 weeks of age. α-Tubulin, loading control. (**G**) Quantification of results shown in **E** and **F**. Striatum, 8 weeks: n = 4–5 mice/genotype; 10 weeks: n = 3 mice/genotype; #2 R6/2 is an outlier excluded from data analyses. 12 weeks: n = 3 mice/genotype. Cortex, 12 weeks: n = 3–4 mice/genotype. Data are represented as mean ± SEM. *P < 0.05; **P < 0.01, unpaired t test.

tion induced a downregulation of total *HTT* mRNA in Q109n1 neurons that was not observed with GFP expression (Figure 3E). We also observed that levels of m-ADAM10 and N-CAD CTF were restored almost up to physiological levels in Q109n1 neurons infected with ZFP-A, while infection with a GFP vector was ineffective (Figure 3, A–D). These experiments indicate that the observed increased m-ADAM10 and N-CAD levels in HD human neurons are directly dependent on the expression of mutant HTT.

Administration of the ADAM10 synthetic inhibitor GI254023X rescues synaptic functional defects in HD mice. We next determined whether normalizing ADAM10 rescues N-CAD cleavage and electrophysiological synaptic phenotypes in HD mice. To this end, we employed GI254023X, a selective hydroxamate inhibitor that chelates the Zn²⁺ of the protease active site and has been used successfully in the past to block ADAM10 catalytic activity in vitro in mammalian cells and in vivo in zebrafish (14, 24). We further confirmed GI254023X specificity for ADAM10 versus ADAM17 by in vitro enzymatic assay with a fluorogenic ADAM substrate showing it possesses 122.4-fold increased selective inhibitory potency for ADAM10 (IC_{50} = 13.67 nM) compared with ADAM17 (IC_{50} = 1673 nM). As GI254023X does not pass the

blood-brain barrier (BBB), we acutely exposed corticostriatal brain slices from 11-week-old control and R6/2 mice to increasing doses of compound for 45 minutes. GI254023X at a concentration of 1, 10, 100, and 1000 nM was able to significantly prevent the excessive production of the N-CAD CTF in R6/2 brain slices compared with R6/2 vehicle-treated slices (Figure 4, A and B). To test the functional effect of ADAM10 inhibition at the HD excitatory synapses, we incubated acute brain slices from 11-week-old R6/2 and heterozygous 54-week-old zQ175 mice in the presence of 50 nM GI254023X for 45 minutes, followed by whole-cell patch clamp to record basic membrane properties and spontaneous excitatory post-synaptic currents (sEPSCs) in MSNs. As previously shown (25, 26), we confirmed that membrane capacitance (C_m) is reduced, input resistance (R_{in}) increased, and membrane resting potential (V_m) depolarized in R6/2 and zQ175 MSNs compared with WT MSNs, reflecting smaller cell size and abnormal ion channel expression in HD MSNs (Supplemental Figure 6, A–F, and Supplemental Table 1). Upon GI254023X administration, these parameters remained unchanged (Supplemental Figure 6, A–F, and Supplemental Table 1). We conclude that GI254023X does not change the cell size, ion channel expression, and/or activity on the
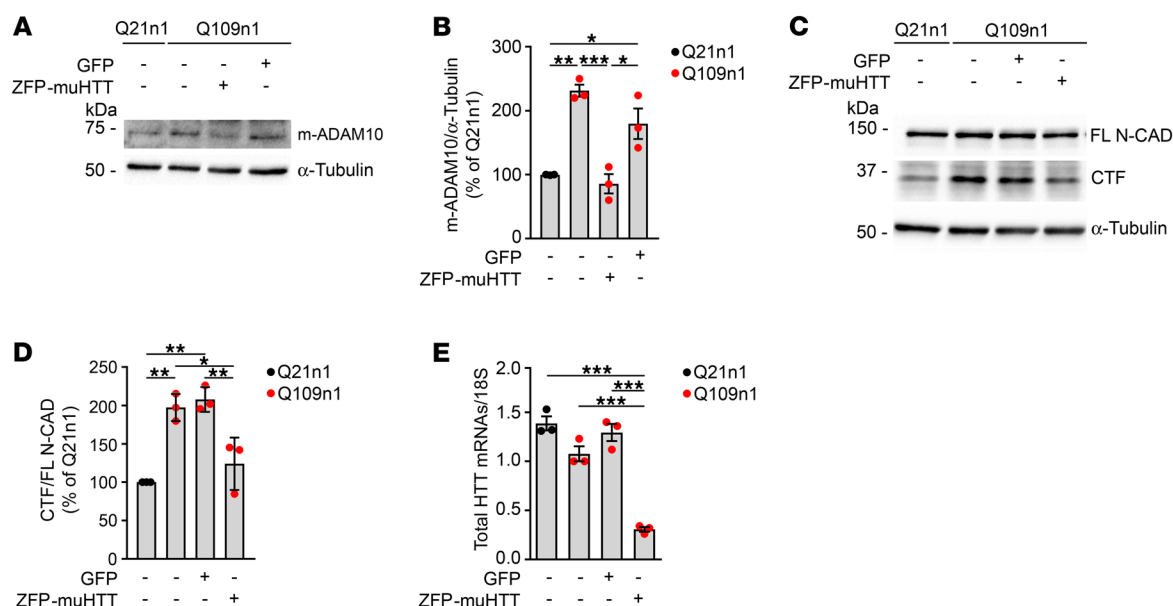
Figure 3. Mutant HTT suppression prevents increased levels of m-ADAM10 and N-CAD proteolysis in human HD neurons. Control (Q21n1) and HD (Q109n1) iPS cells were exposed to neuronal differentiation. A synthetic ZFP targeting mutant HTT (ZFP-muHTT) was delivered to Q109n1 at DIV20 and DIV23, and GFP was used as control. Levels of m-ADAM10, N-CAD CTF, and *HTT* mRNA were analyzed at DIV30 of neuronal differentiation. (**A**) Representative Western blot for m-ADAM10 in neurons generated from Q21n1 and Q109n1 iPS cells infected with ZFP-muHTT and GFP. α-Tubulin, loading control (**B**) Quantification of data in **A**. *$P < 0.05$; **$P < 0.01$; ***$P < 0.001$, 1-way ANOVA followed by Bonferroni's post hoc test. (**C**) Representative Western blot for N-CAD CTF in neurons from Q21n1 and Q109n1 iPS cells infected with ZFP-muHTT and GFP. α-Tubulin, loading control. (**D**) Quantification of data in **C**. *$P < 0.05$; **$P < 0.01$, 1-way ANOVA with Bonferroni's post hoc test. (**E**) qPCR for total *HTT* mRNA in neurons from Q21n1 and Q109n1 iPS cells infected with ZFP-muHTT and GFP. ***$P < 0.001$, 1-way ANOVA with Bonferroni's post hoc test. Data are represented as mean ± SEM of $n = 3$ technical replicates.

plasma membrane. As reported previously (25, 26), the spontaneous glutamatergic synaptic activity of MSNs is affected, and with HD progression, the sEPSC frequency, but not amplitude, is reduced in R6/2 and zQ175 MSNs compared with WT MSNs (Figure 4, C and D, Supplemental Figure 7, A and B, and Supplemental Table 2). When GI254023X was applied to both R6/2 and zQ175 brain slices, a significant rescue of sEPSC frequency occurred compared with that in untreated R6/2 and zQ175 MSNs (Figure 4, C and D). sEPSCs may be produced by the release of synaptic vesicles (SVs) following either the arrival of a spontaneous action potential at the presynaptic terminal or by stochastic SVs release. By applying the Na⁺ channel blocker tetrodotoxin (TTX), we could measure action potential–independent postsynaptic events defined miniature EPSCs (mEPSCs), the frequency of which reflects the presynaptic probability of releasing SVs and is also correlated to the number of synapses. We found that mEPSC frequency was reduced in R6/2 MSNs compared with WT MSNs (Figure 4E). Notably, treatment with GI254023X determined a significant rescue in mEPSC frequency of R6/2 MSNs compared with untreated R6/2 MSNs (Figure 4E), consistent with ADAM10 inhibition acting presynaptically to increase the probability of presynaptic vesicles release. mEPSC amplitude, which is an indicator of postsynaptic responsiveness, was not affected in R6/2 MSNs before and after treatment (Supplemental Figure 7C and Supplemental Table 3), indicating that the quantal size, the number and structure of postsynaptic receptors, and the location of synaptic contacts are not affected by mutant HTT, nor by GI254023X. Collectively, these data indicate that inhibition of ADAM10 activity improves functional deficits of the excitatory HD synapse.

TAT-Pro-ADAM10$^{709–729}$ *peptide prevents N-CAD proteolysis and cognitive decline in HD mice*. Binding of ADAM10 to synapse associated protein 97 (SAP97) is required for inserting ADAM10 into the synaptic membrane (27). SAP97 promotes ADAM10 trafficking at the excitatory synapse by a direct interaction between its Src homology 3 (SH3) domain and the proline-rich domains of ADAM10 (27). We investigated whether reducing synaptic trafficking of ADAM10 by disrupting the ADAM10/SAP97 complex could prevent N-CAD cleavage and synaptic phenotypes in R6/2 mice (27, 28). To this end, we employed a cell-permeable peptide (TAT-Pro-ADAM10$^{709–729}$) that contains the proline-rich domain of ADAM10 and competes with endogenous ADAM10 for the binding to SAP97 (28). As a control, animals were injected with the TAT-Ala-ADAM10$^{709–729}$ peptide, which is unable to bind SAP97 because prolines are substituted by alanines. WT and R6/2 mice at 12 weeks of age received 2 i.p. injections 24 hours apart of either TAT-Pro-ADAM10$^{709–729}$ or TAT-Ala-ADAM10$^{709–729}$ peptide (2 nmol/g) diluted at 0.5 mg/ml in sterile saline solution (Figure 5A). We found that i.p. injection of the TAT-Pro-ADAM10$^{709–729}$ in 12-week-old R6/2 mice reduced levels of synaptic m-ADAM10 compared with TAT-Ala-ADAM10$^{709–729}$–treated mice (Figure 5, B and C). Moreover, Western blots revealed that TAT-Pro-ADAM10$^{709–729}$ was effective in reducing the excessive levels of N-CAD CTF in the R6/2 striatum (Figure 5, D and E) and cortex (Figure 5, F and G), while the control peptide had no effect (Figure 5, D–G). We then employed the cued fear conditioning test to evaluate whether treatment with TAT-Pro-ADAM10$^{709–729}$ could improve cognitive experience in R6/2 mice. On day 1, animals were trained to associate conditioned stimuli (CS, environment and
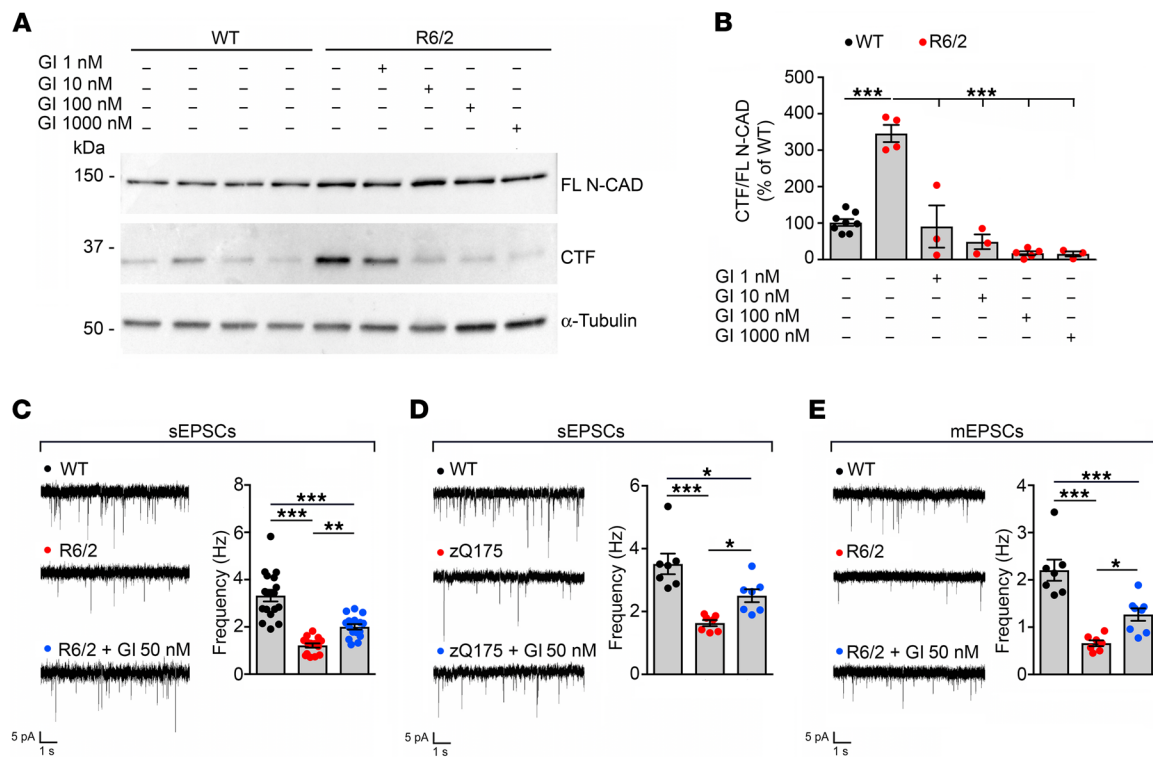
Figure 4. Treatment with the ADAM10 inhibitor GI254023X reduces N-CAD proteolysis and rescues electrophysiological defects of the excitatory synapse in HD. (**A**) Representative Western blot for N-CAD on corticostriatal brain slices from 4 untreated 11-week-old WT mice and 1 R6/2 mouse acutely treated with vehicle and GI254023X at concentrations of 1, 10, 100, and 1000 nM. α-Tubulin, loading control. (**B**) Quantification of data shown in **A**. WT, $n = 8$; R6/2 treated with GI254023X or vehicle, $n = 3$–5. ***$P < 0.001$, 1-way ANOVA with Bonferroni's post hoc test. (**C**) sEPSCs frequencies recorded from striatal MSNs of WT and R6/2 mice at 11 weeks of age. WT, $n = 17$; R6/2-untreated, $n = 15$; R6/2-GI254023X-50nM, $n = 16$. **$P < 0.01$; ***$P < 0.001$, 1-way ANOVA with Bonferroni's post hoc test. (**D**) sEPSC frequencies recorded from striatal MSNs of WT and zQ175 mice at 54 weeks of age. WT, $n = 7$; zQ175-untreated, $n = 7$; zQ175-GI254023X-50nM, $n = 7$. *$P < 0.05$; *** $P < 0.001$, 1-way ANOVA with Bonferroni's post hoc test. (**E**) mEPSC frequencies recorded from striatal MSNs of WT and R6/2 mice at 11 weeks of age. WT, $n = 7$; R6/2-untreated, $n = 7$; and R6/2-GI254023X-50nM, $n = 8$. *$P < 0.05$; ***$P < 0.001$, 1-way ANOVA with Bonferroni's post hoc test. Data are represented as mean ± SEM.

acoustic tone), with an aversive stimulus (AS, electric foot shock). On day 2, animals were left in their housing rooms to rest, and on day 3 they were exposed to a different environment in the presence of the sole acoustic tone (cued stage). In cued stage, mice generally demonstrate a freezing response if they remember and associate the acoustic tone with the AS. Latency to freeze was longer with R6/2-TAT-Ala-ADAM10[709–729] in cued stage compared with WT-TAT-Ala-ADAM10[709–729] (Figure 5H), indicating that R6/2 mice require a longer time to associate the CS with the AS. In line with these data, a shorter freezing time was found with R6/2-TAT-Ala-ADAM10[709–729] in cued stage (Figure 5I), confirming that R6/2 mice fail to remember an association between CS and AS. Notably, R6/2-TAT-Pro-ADAM10[709–729] mice exhibited a shorter latency to freeze than R6/2-TAT-Ala-ADAM10[709–729] and a longer freezing time in cued stage (Figure 5, H and I). Together, these data suggest that reduction of ADAM10 trafficking to the postsynaptic compartment alleviates cognitive impairments in HD mice.

Genetic reduction of ADAM10 corrects synaptic loss and cognitive decline in R6/2 mice. To further evaluate the therapeutic potential of ADAM10 inhibition in HD, we crossed R6/2 mice with *CaMKIIα-Cre:Adam10[Flox/+]* mice (A10cKO), an ADAM10 heterozygous conditional KO mouse line limiting ADAM10 inactivation to the postnatal forebrain, to obtain R6/2-A10cKO mice

(Figure 6A) (10). Western blot showed that synaptic m-ADAM10 (Figure 6, B and C) and N-CAD CTF levels (Figure 6, D and E) in R6/2-A10cKO striatum were fully restored to the amount that is found in WT animals. Synapse loss correlates robustly with cognitive decline in HD patients and HD animal models (29, 30). To determine whether ADAM10 inhibition prevents synapse loss, we examined the excitatory synapse density in striatal sections by using serial block-face scanning electron microscopy (SBF-SEM) imaging and high-resolution 3D reconstruction of the synapse. Our blinded ultrastructural analyses revealed 28% loss of striatal glutamatergic synapses in 13-week-old R6/2 mice compared with controls (Figure 6, F, G, and J), which was rescued by ADAM10 heterozygous deletion in R6/2-A10cKO mice (Figure 6, H and J). The number of glutamatergic synapses was not affected in A10cKO mice (Figure 6, I and J). We then used transmission electron microscopy (TEM) to examine pre- and postsynaptic densities (PSDs), which are located at the heads of spines and are critical for synaptic function. In line with electrophysiological data, our TEM morphological analyses revealed that, although postsynaptic parameters were not affected (Supplemental Figure 8, A and B), SVs density and number of docked vesicles were decreased in R6/2 presynaptic compartment (Figure 6, K and L). Notably, these structural deficits were rescued by heterozygous
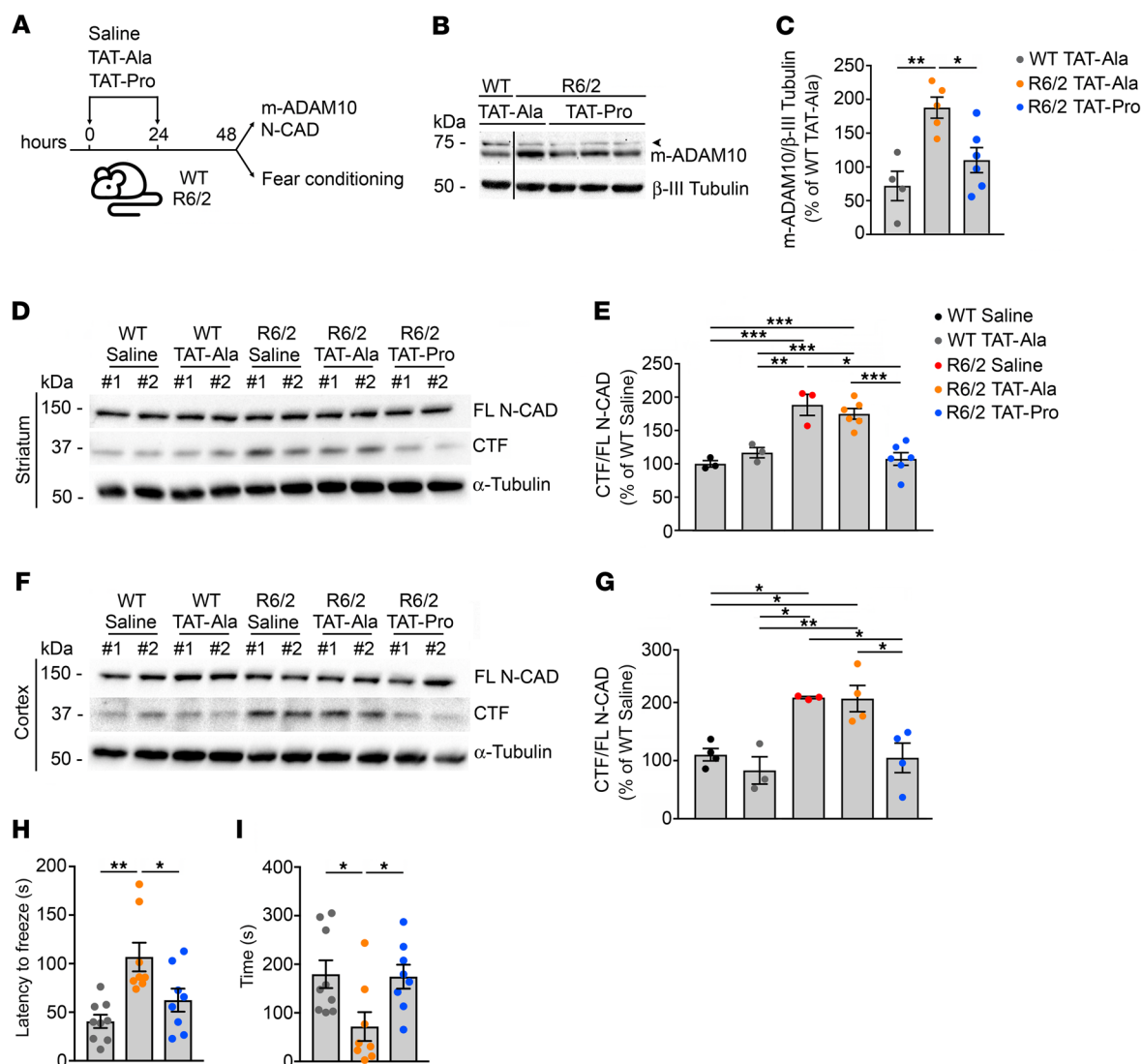
Figure 5. TAT-Pro-ADAM10[709–729] peptide normalizes N-CAD proteolysis and rescues cognitive deficits in R6/2 mice. (**A**) TAT-Pro-ADAM10[709–729] (TAT-Pro) interferes with ADAM10/SAP97 interaction and impairs ADAM10 synaptic trafficking. TAT-Ala-ADAM10[709–729] (TAT-Ala), inactive peptide. 12-week-old WT and R6/2 mice received 2 i.p. injections of TAT-Pro or TAT-Ala at 2 nmol/g 24 hours apart. Saline solution, vehicle. Synaptic level of m-ADAM10, N-CAD proteolysis, and cognitive function were monitored 24 hours after the second i.p. injection. (**B**) Representative Western blot for m-ADAM10 in striatal synaptic fractions of 12-week-old WT and R6/2 mice treated with TAT-Pro or TAT-Ala. β-III Tubulin, loading control. Arrowhead, nonspecific band. Lanes were run on the same gel, but were noncontiguous. (**C**) Quantification of data in **B**. WT-TAT-Ala, $n = 4$; R6/2-TAT-Ala, $n = 5$; R6/2-TAT-Pro, $n = 6$. *$P < 0.05$; **$P < 0.01$, 1-way ANOVA with Bonferroni's post hoc test. (**D**) Representative Western blot showing effects of TAT peptides on N-CAD proteolysis in the striata of R6/2 mice. α-Tubulin, loading control. (**E**) Quantification of data in **D**. WT-saline, $n = 3$; WT-TAT-Ala, $n = 3$; R6/2-saline, $n = 3$; R6/2-TAT-Ala, $n = 6$; R6/2-TAT-Pro, $n = 6$. *$P < 0.05$; **$P < 0.01$; ***$P < 0.001$, 1-way ANOVA with Bonferroni's post hoc test. (**F**) Representative Western blot showing effects of TAT peptides on N-CAD proteolysis in the cortices of R6/2 mice. α-Tubulin, loading control. (**G**) Quantification of data shown in **F**. WT-saline, $n = 4$; WT-TAT-Ala, $n = 3$; R6/2-saline, $n = 3$; R6/2-TAT-Ala, $n = 4$; R6/2-TAT-Pro, $n = 4$. *$P < 0.05$; **$P < 0.01$, 1-way ANOVA with Bonferroni's post hoc test. (**H**, **I**) Effect of TAT peptides in the fear conditioning test in WT and R6/2 mice at 12 weeks of age. WT-TAT-Ala, $n = 9$; R6/2-TAT-Ala, $n = 8$; R6/2-TAT-Pro, $n = 8$. Cued fear response evaluated as latency to freeze (**H**) and freezing time (**I**). *$P < 0.05$; **$P < 0.01$, 1-way ANOVA with Newman-Keuls. Data are represented as mean ± SEM.

suppression of the ADAM10 gene (Figure 6, K and L). Taken together, these data indicate that reduced synapse density and presynaptic pathology in HD are due to increased ADAM10 activity. To validate the effect of ADAM10 inhibition on HD cognitive phenotypes, WT, R6/2, R6/2-A10cK10, and A10cKO mice were tested by contextual and cued fear conditioning. We found that 9-week-old and 13-week-old R6/2 mice require a longer time to associate the CS (environment and acoustic tone) with the AS

(electric foot shock) because their latency to freeze was higher in both the contextual (Figure 6M) and cued stages (Figure 6N) compared with control groups (WT and A10cKO). In line with these data, a shorter freezing time was found in R6/2 mice under both conditions, which became significant at the cued stage (Figure 6, O and P). In contrast, 9-week-old and 13-week-old R6/2-A10cKO mice showed a significantly shorter latency to freeze than R6/2 mice at both the contextual (Figure 6M) and cued stag-
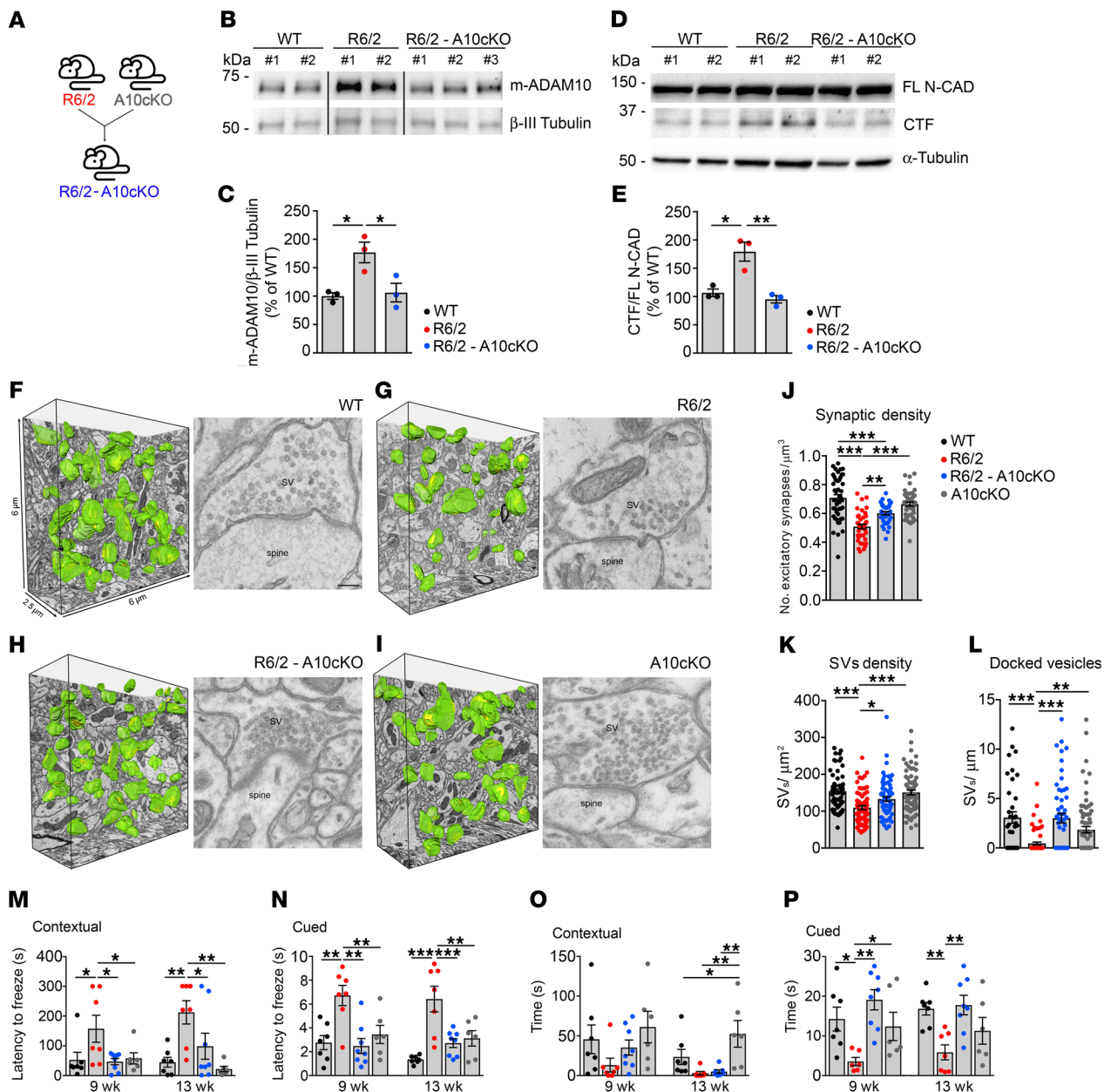
Figure 6. ADAM10 heterozygous deletion in the forebrain rescues synapse loss and cognitive decline in R6/2 mice. (**A**) *CaMKIIα-Cre:Adam10^Flox/+*(A10cKO) mice were crossed with R6/2 to obtain *R6/2:CaMKIIα-Cre:Adam10^Flox/+*(R6/2-A10cKO). (**B**) Representative Western blot for synaptic m-ADAM10 in the striata of WT, R6/2, and R6/2-A10cKO at 13 weeks of age. β-III Tubulin, loading control. Lanes were run on the same gel, but were noncontiguous. (**C**) Quantification of data in **B**. $n = 3$ mice/genotype, $*P < 0.05$, 1-way ANOVA with Bonferroni's post hoc test. (**D**) Western blot of CTF N-CAD in the striata of WT, R6/2, and R6/2-A10cKO at 13 weeks of age. α-Tubulin, loading control. (**E**) Quantification of data in **D**. $n = 3$ mice/genotype. $*P < 0.05$; $**P < 0.01$, 1-way ANOVA with Bonferroni's post hoc test. (**F–I**) Representative SBF-SEM segmentation and reconstruction of excitatory synapses (green) with their PSD (yellow) in 90 μm^3 of striatum, and TEM images of striatal synaptic profile of WT (**F**), R6/2 (**G**), R6/2-A10cKO (**H**), and A10cKO (**I**) mice at 13 weeks of age. Scale bar: 100 nm. (**J**) Quantification of excitatory synapse density in 800 μm^3 of striatal tissue/mouse in $n = 3$ mice/genotype. $**P < 0.01$; $***P < 0.001$, 1-way ANOVA with Bonferroni's post hoc test. (**K**) Quantification of SVs density and (**L**) docked vesicles/μm AZ in $n = 3$ mice/genotype. At least $n = 60$ excitatory synapses/genotype were analyzed. $*P < 0.05$; $**P < 0.01$; $***P < 0.001$, 1-way ANOVA with nonparametric Dunn's multiple comparison test. (**M–P**) Fear conditioning test on WT, R6/2, R6/2-A10cKO, and A10cKO mice at 9 and 13 weeks of age. $n = 6$–8 mice/genotype. (**M**, **N**) Contextual and cued fear responses evaluated as latency to freeze and (**O**, **P**) freezing time. $*P < 0.05$; $**P < 0.01$; $***P < 0.001$, 1-way ANOVA with Newman-Keuls post hoc test. Data are represented as mean ± SEM.

es (Figure 6N) and a longer freezing time at the cued stage (Figure 6P). No improvement in RotaRod performance was observed in R6/2-A10cKO mice (Supplemental Figure 9). Taken together, these data indicate that increased ADAM10 activity in HD contributes to cognitive but not to motor decline.

Discussion

Although HD has been classically considered as a neurodegenerative disorder characterized by voluntary movement, cognitive decline is now receiving increased attention, as it is highly invalidating for the patients. Considerable efforts have been invested

to determine which components of the altered corticostriatal synapse contribute to cognitive deficits. Preclinical research revealed that some available compounds attenuate synaptic dysfunction and cognitive decline in HD mouse models, but human trials have been so far disappointing, demonstrating little or no therapeutic benefits and substantial side effects.

Here, we propose ADAM10 as a target of interest in HD due to its inherent structural and functional role in synaptic connectivity. Our study reveals that overabundance of active ADAM10 and, as a consequence, the proteolysis of the synaptic cell adhesion protein N-CAD, mediates mutant HTT-associated synaptic and cognitive dysfunction. In the HD brain, active ADAM10 accumulates at the PSDs and causes excessive N-CAD cleavage. These molecular events determine loss of excitatory synaptic contacts and reduce the density of presynaptic vesicles and the number of vesicles ready for release, ultimately leading to excitatory synapse deficiencies and cognitive decline in HD. Relevant to the disease, we found that the level of active ADAM10 is also increased in the human HD caudate tissues and in HD neurons generated from iPS cells, the latter phenotype being reverted by selective suppression of mutant HTT. These findings suggest that, similar to the mouse model, increased ADAM10 activity may also have a detrimental effect on synaptic structure and function in patients. Future studies are needed to determine whether increased ADAM10 activity is strictly related to synaptic dysfunction or whether it contributes to other disease phenotypes. Identifying novel ADAM10 interactors and substrates may help in deciphering the impact of ADAM10 on HD pathogenesis.

Our data also suggest that molecular, pharmacological, and genetic targeting of the ADAM10 can be neuroprotective in HD. Therapeutic targeting of ADAM10 with the hydroxamate inhibitor GI254023X is able to reduce excessive N-CAD proteolysis in the striatum ex vivo and to correct electrophysiological defects in MSNs from 2 HD mouse models. Consistently, normalizing ADAM10 activity in the HD brain by in vivo delivery of a competitive TAT-Pro-ADAM10[709-729] peptide alleviates cognitive decline in HD mice. We further validated our findings by showing that conditional heterozygous deletion of ADAM10 in the forebrain prevents synapse loss and synaptic ultrastructural defects in the striatum of HD mice, reducing cognitive impairment.

Our ex vivo and in vivo evidence suggests that safe, selective, and brain-penetrant peptides or drug-like molecules specifically designed to interfere with ADAM10 deserve to be explored in HD. Although 50% genetic ablation of ADAM10 in the forebrain is well tolerated in WT mice, the doses of ADAM10 inhibitors and therapeutic windows of application have to be defined carefully in order to preserve a physiological concentration of the active enzyme (31). Caution is needed because a reduction in ADAM10 activity below 50% causes severe disruption of synaptic architecture and function and increased formation of Aβ peptides in mice (10). ADAM10 is expressed almost ubiquitously in the body and plays important roles in peripheral tissues beyond the brain (9). Selectively targeting the ADAM10/SAP97 complex in the HD brain could finely tune ADAM10 shedding activity toward N-CAD, overcoming problems and unwanted side effects related to systemic inhibition of the protease.

In summary, our findings indicate that interfering with ADAM10 activity may be a powerful strategy for preventing synaptic dysfunction and cognitive decline in HD. We also speculate that destabilization of the synaptic cell adhesion contacts by increased ADAM10 activity could render the HD synapses unstable and less responsive to drugs, especially those acting on neurotransmitters and receptor systems impaired in the disease (32). Increased ADAM10 activity in HD and the consequently disrupted synaptic structure may help explain why these drugs have so far been largely inefficacious in clinical trials.

Methods

Human tissues. All postmortem human tissue was obtained from the Harvard Brain Tissue Resource Center (HBTRC) (Belmont, Massachusetts, USA). Patient information is present in Table 1.

Rodent models. WT and R6/2 mice (B6CBAF1/J) were purchased from the Jackson Laboratory (15). Heterozygous *Adam10* floxed mice (*Adam10[Flox/+]*) (C57BL/6J × 129 S6) and *CaMKIIalpha-Cre* recombinase transgenic mice (C57BL/6J × 129 S6) were generated as described before (10). Brain tissues from WT and zQ175 (C57BL/6J) mice were obtained from the CHDI Foundation (16). SCA3 mice (B6-Tg(Prnp-ATXN3*)71-OR/OR), SCA17 mice (B6CBA(FVB)-Tg(Prnp-TBP*)71-16Xjl/J), and SCA17 rats (Crl:CD(SD)-Tg(Prnp-TBP*)64-HPN/HPN) were generated as described before (17–19). Both male and female mice were used for biochemical and behavioral analyses.

Cell lines. HEK293T cells (ATCC) were maintained in DMEM (Gibco, Thermo Fisher Scientific, catalog 31885-023) supplemented with 10% FBS (Gibco Thermo Fisher Scientific, catalog 10270-106) and 1% penicillin/streptomycin (Gibco Thermo Fisher Scientific, catalog 15140-122). Nonintegrating HD (Q109n1) and control (Q21n1) iPS cell lines were generated in the C. Svendsen laboratory at Cedars-Sinai Medical Center (33). The lines/clones used in this study were regularly tested for karyotype and maintained as mycoplasma free. iPS cells were maintained in mTeSR1 medium (STEMCELL Technologies, catalog 85850) and plated on Matrigel (Trevigen, catalog 3434-001-02).

Neuronal differentiation of iPS cells. Cells were plated at a density of 0.6×10^5 cells/cm² on Matrigel-coated dishes in mTeSR1 with 10 μM ROCK inhibitor (MilliporeSigma, catalog Y-27632). Cultures were expanded for 2 days until cells reached 70% confluency. DMEM/F12 (Gibco, Thermo Fisher Scientific, catalog 11320033) supplemented with N2 and B27 (Gibco, Thermo Fisher Scientific, catalog 17502048 and 17504044), 10 μM SB431542, and 500 nM of LDN (provided by Evotec) were used as starting differentiation medium. Medium was replaced every day. At day 15, the cells were detached by Accutase (MilliporeSigma, catalog SF006) and replated on Matrigel at a density of 2.5×10^4 cells/cm². The cells were differentiated in terminal differentiation medium by adding 30 ng/mL BDNF (PrepoTech, catalog 450-02) together with N2 and B27.

ZFPs cloning strategy and iPS cell infection. The coding sequences for the ZFP-A repressor were cut from the previously described FUW-tetO-ZFP plasmids using the restriction enzymes AfeI and NheI (23). The sequences were then subcloned into the lentiviral plasmid pLV-hSyn-RFP (Addgene, catalog 22909) by replacing the RFP sequence through compatible digestion with restriction enzymes PmeI and XbaI. iPS cells were differentiated as described above and infected or not twice with the lentiviral supernatant coding for ZFP-A or GFP at DIV20 and 23 using 5 μl/well in 12-well plates. The viruses were diluted in 1 ml terminal differentiation medium with 4 μg/ml polybrene (MilliporeSigma, cata-

log TR1003-G), and cells were exposed for 18 hours. At DIV30, infected and untreated cells were detached using Accutase (EMD Millipore, catalog SF006) and centrifuged for 3 minutes at 8000 g for storage at –80°C.

Lentivirus production. HEK293NT cells (ATCC) were used for viral production and cultured in DMEM (Gibco, Thermo Fisher Scientific, catalog 31885-023) supplemented with 10% FBS (Gibco, Thermo Fisher Scientific, catalog 10270-106), 0,5% penicillin/streptomycin (Gibco, Thermo Fisher Scientific, catalog 15140-122), 2 mM glutamine (Euroclone, catalog ECB3000D), 1 mM sodium pyruvate (Gibco, Thermo Fisher Scientific, catalog 11360-039), and 1% nonessential amino acids (Gibco, Thermo Fisher Scientific, catalog 11140-035). For the production of lentiviral supernatants for the pLV-hSyn-ZFP-A and pLV-hSyn-GFP constructs, cells were plated on gelatin-coated dishes at a density of 45,000 cells/cm² and were transfected on the following day with Lipofectamine 3000 (Invitrogen, Thermo Fisher Scientific, catalog L300-015) according to the manufacturer's instructions. The single donor plasmid was cotransfected with the third generation packaging vectors pMDLg/pRRE (Addgene, catalog 12251), pRSV-Rev (Addgene, catalog 12253), and pMd2.G (Addgene, catalog 12259) at a 4:2:1:1 ratio, respectively. The transfection mix was removed after overnight incubation, and fresh medium was supplied to the cells. The supernatant was collected 48 hours and 72 hours after transfection and centrifuged at 60,000 g for 2 hours; concentrated viral particles were resuspended in PBS and stored at –80°C.

HD mice genotyping. Genotyping of R6/2 (B6CBAF1/J) and zQ175 (C57BL/6J) mouse colonies (~150 CAG and 175 repeats, respectively) was performed by PCR of genomic DNA obtained from tail samples (Nucleo Spin Tissue, Macherey-Nagel, catalog 740952.250) at weaning and following sacrifice for verification. CAG repeats of R6/2 mice were sized by using the following PCR primers: forward: ATGAAGGCCTTCGAGTCCCTCAAGTCCTTC; reverse: GGCGGCTGAGGAAGCTGAGGA. Cycling conditions were 94°C for 90 seconds, 35 cycles × (94°C for 60 seconds, 65°C for 45 seconds, 72°C for 60 seconds), 72°C for 7 minutes. CAG repeats of zQ175 mice were sized by using the following PCR primers: forward: CATTCATTGCCTTGCTGCTAAG; reverse: CTGAAACGACTTGAGCGACTC. Cycling conditions were 94°C for 10 minutes, 30 cycles × (96°C for 30 seconds, 57°C for 30 seconds, 72°C for 30 seconds), 72°C for 7 minutes.

Treatment of mice with TAT peptides. WT and R6/2 mice at 12 weeks of age received 2 i.p. injections 24 hours apart of either TAT-Pro-ADAM10[709–729] (2 nmol/g) or TAT-Ala-ADAM10[709–729] peptide (2 nmol/g) diluted at 0.5 mg/ml in sterile saline solution. The cell-permeable peptide TAT-Pro-ADAM10[709–729] was obtained by linking the 11 amino acids of the human immunodeficiency virus TAT transporter sequence to the 21 amino-acid sequence corresponding to ADAM10 proline-rich domains (NH2-YGRKKRRQRRRPKLPPPKPLPGTLKRR-RPPQP-COOH). TAT-Ala-ADAM10[709–729] peptide, in which all proline residues were mutated into alanine (NH2-YGRKKRRQRRRAK-LAAAKALAGTLKRRRAAQA-COOH), was used as control (27, 28). The TAT-Pro-ADAM10[709–729] inhibitory peptide and TAT-Ala-ADAM10[709–729] control peptide were generated by PolyPeptide and were maintained at 4°C while lyophilized. Once solubilized, solutions were maintained at –20°C for a maximum of 1 week. For biochemical analyses, animals were euthanized 24 hours after the second injection by dislocation and the brains were rapidly removed for dissection of stri-

atal and cortical tissues. For behavioral analysis, mice were tested for the fear-conditioning test 24 hours after the second injection.

Generation of R6/2-A10cKO mice. R6/2 mice (B6CBAF1/J) were generated by crossing R6/2 males with WT females (B6CBAF1/J). The A10cKO colony was maintained by crossing heterozygous floxed mice (*Adam10[Flox/+]*) (C57BL/6J × 129 S6) with *CaMKIIalpha*-Cre recombinase transgenic mice (C57BL/6J × 129 S6). A10cKO exhibited a normal phenotype and a normal fertility. From the crossing between heterozygous A10cKO and R6/2 mice, we tested 4 genotypes of the F1, including WT, R6/2, R6/2-A10cKO, and A10cKO, which are on the same mixed genetic background. Mice were genotyped as previously described (10).

Behavioral tests. Motor and cognitive functions were assessed by the same operator blinded to the treatment. A group of animals was tested at 6, 10, and 12 weeks of age for the assessment of the motor behavior by the RotaRod test. Another group of animals was tested at 9 and 13 weeks of age for the assessment of cognitive deficits by the fear conditioning test. For RotaRod, the test was performed using the accelerating RotaRod apparatus (Ugo Basile, catalog 47600). Mice were moved to the RotaRod room at least 30 minutes before starting the test. Mice were tested 2 days a week. On each testing day, mice were first trained at a constant speed of 4 rpm for 5 minutes on the apparatus. Mice were then tested in 3 consecutive sessions with acceleration from 4 to 40 rpm in 5 minutes. The time at which mice fell from the rotating bar was recorded, for a maximum of 5 minutes. The best performance of each day was recorded, and the average between the 2 trials was reported in the graph. Contextual and cued fear conditioning was performed using the Fear Conditioning System (Ugo Basile, series 46000). WT-TAT-Ala-ADAM10[709–729], R6/2-TAT-Ala-ADAM10[709–729], and R6/2-TAT-Ala-ADAM10[709–729] mice were tested by cued fear conditioning according to the following protocol: on day 1, mice were transferred to the behavioral room at least 30 minutes before starting the test. The conditioned stimulus (CS) was a 10-second 3.5 kHz tone delivered 150 seconds after the beginning of the test. The unconditioned stimulus (US) was a 2-second 0.5 mA footshock that coterminated with the CS. The conditioning was repeated 3 times, every 150 seconds. After the last conditioning, animals were let in the same chamber for 150 seconds, and then they were placed in their cage. During day 2, animals were left in their housing room to rest. On day 3, cued fear conditioning was assessed using a modified conditioning chamber obtained by attaching patterned contexts on the walls and floor. Once mice were placed in this modified chamber, a protocol similar to that of day 1 was applied, except for the electrical footshock that was not administered. Freezing of animals was assessed and recorded during the tone activation in order to focus the analysis during the CS. Latency to freeze and time of freezing were recorded. WT, R6/2, R6/2-A10cKO, and A10cKO mice were tested by contextual and cued fear conditioning according to the following protocol: on day 1, mice were trained as described above for WT and R6/2 mice treated with TAT peptides. On day 2, contextual memory was assessed by placing animals in the same conditioning chamber for 5 minutes and measuring freezing response in terms of time of freezing and latency to freeze. On day 3, cued fear conditioning was assessed as described above for WT and R6/2 mice treated with TAT peptides.

Western blot for iPS cells and mouse and human tissue. Samples were lysed in RIPA buffer (50 mM Tris-HCl pH 8, 150 mM NaCl, 0.1% SDS, 1% Nonidet P40, 0.5% sodium deoxycholate) with 1 mM PMSF and 1× protease inhibitor cocktail (Thermo Scientific, catalog 1861281). Lysates were cleared by centrifugation for 30 minutes at 12,000 g and

4°C. The resulting supernatant was collected. Protein concentration was determined with the BCA assay (Thermo Fisher Scientific, catalog 23225) and 20–60 μg was loaded on a 10% SDS-PAGE gel. Separated proteins were transferred onto a nitrocellulose membrane (Bio-Rad Turbo Nitrocellulose, catalog 1704158) by means of the Trans-blot Turbo Transfer System (Bio-Rad) (standard protocol: 1.5 A constant; up to 25 V; 10 minutes), blocked with 5% nonfat dry milk (Bio-Rad, catalog 1706404) in TBS and 0.1% Tween 20 (TBST), and incubated with primary antibodies at room temperature for 3 hours or at 4°C overnight. After washing, filters were incubated for 1 hour at room temperature with a peroxidase conjugate secondary antibody (1:3000; Bio-Rad, goat anti-rabbit HRP, catalog 1706515, goat anti-mouse HRP, catalog 1706516) and then washed 3 times with TBS and 0.1% Tween 20. The Clarity Western ECL Substrate (Bio-Rad, catalog 1705061) was used to visualize immunoreactive bands. Blot visualization was performed by using the ChemiDoc MP Imaging System from Bio-Rad. Densitometric analyses were performed by using Image Lab 4.1 software. The primary antibodies and dilutions used for the Western blot were as follows: mouse monoclonal anti–N-CAD (1:1000; Becton Dickinson Transduction Laboratories, catalog 610921); mouse monoclonal anti α-Tubulin (1:5000; MilliporeSigma, catalog T9026); rabbit polyclonal anti-ADAM9 (1:1000; Enzo Life Science, catalog SA-376); rabbit polyclonal anti-ADAM10 and anti-ADAM17 (1:1000; provided in house). The ADAM10 antibody was validated by using ADAM10-knockout brain tissues: a 75 kDa nonspecific signal was revealed.

Isolation of TIF and synaptosomes. For the isolation of TIF-PSD fractions from striatal and cortical tissues of WT and R6/2 at 6 and 12 weeks of age, mouse tissue homogenization was carried out by 10 strokes in a Teflon-glass homogenizer (clearance 0.25 mm, 700 rpm) in 4 ml/g wet weight cold 0.32 M sucrose solution containing 1 mM Hepes pH 7.4, 1 mM MgCl$_2$, 1 mM EDTA pH 8, 1 mM NaHCO$_3$, 0.1 mM PMSF, and 1× protease inhibitors (Thermo Fisher Scientific, catalog 1861281). The homogenized tissue was centrifuged at 2,300 *g* for 10 minutes at 4°C. The resulting supernatant was centrifuged at 13,000 *g* for 30 minutes at 4°C, and the pellet was resuspended in a solution of 75 mM KCl, 1% Triton X-100, 0.1 mM PMSF, and 1× protein inhibitors and centrifuged at 100,000 *g* for 2 hours at 4°C. The pellet was resuspended in 50 mM HEPES pH 7.4 and 5% glycerol. From 20 to 30 μg TIF-PSD enriched fraction was loaded on a 10% SDS-PAGE gel. Separated proteins were transferred onto a nitrocellulose membrane (Bio-Rad Turbo Nitrocellulose, catalog 1704158) by means of the Trans-blot Turbo Transfer System (Bio-Rad) (standard protocol: 1.5 A constant; up to 25 V; 10 minutes), blocked with 5% nonfat dry milk (Bio-Rad, catalog 1706404) in TBS and 0.1% Tween 20, and incubated with primary antibodies at room temperature for 3 hours or at 4°C overnight. The primary antibodies used for Western blot on PSD fractions were as follows: rabbit polyclonal anti-ADAM10 (1:1000; provided in house); mouse monoclonal anti–βIII-Tubulin (1:1000; Promega, catalog G712A); mouse monoclonal anti-PSD95 antibody (1:2000; Thermo Fisher Scientific, catalog 6G6-1C9). Synaptosomes from WT, R6/2, R6/2-A10cKO, and from human postmortem tissues were prepared by using Syn-PER Reagent (Thermo Scientific, catalog 87793) according to the manufacturer's instructions. Samples containing equal amounts of protein lysates were loaded on 10% SDS-PAGE gels, and blots were probed with rabbit polyclonal anti-ADAM10 (1:1000; provided in house) and/or with anti-ADAM10 antibody EPR5622 (1:1000; Abcam, catalog ab124695).

HEK393T transfection and coimmunoprecipitation. cDNAs encoding for human full-length HTT-HA bearing 23 or 83 CAG repeats and for human ADAM10-3XFLAG were synthesized by GenScript and subcloned into pCDNA3.1 vectors. 10 Million cells were transfected with 8 μg of cDNA encoding human HTT and 8 μg of cDNA encoding human ADAM10-3XFLAG or pCDNA3.1 empty vector by using the Lipofectamine 3000 protocol (Invitrogen, Thermo Fisher Scientific, catalog L300-015). Cell pellets were lysed at 48 hours after transfection, using as a lysis buffer PBS containing 0.4% Triton X-100 and 1× protease inhibitor cocktail (Thermo Scientific, catalog 1861281) and centrifuged (12,000 *g* per 15 minutes at 4°C). Supernatant was quantified for total protein content with the BCA method (Thermo Fisher Scientific, Pierce BCA Protein Assay Kit, catalog 23225). Immunoprecipitation was performed using Dynabeads Protein G (Thermo Fisher Scientific, catalog 10004D) according to the manufacturer's instructions. Protein lysate (400 μg) was incubated with 10 μg of mouse monoclonal anti–FLAG-specific antibody (Invitrogen, Thermo Fisher Scientific, catalog MA1-91878) for 1 hour at 4°C on a rotation wheel and then loaded onto 20 μl of Dynabeads (Thermo Fisher Scientific, catalog 10004D) and incubated for 1 hour at room temperature on a rotation wheel. After washing, the beads were eluted in 20 μl/sample of loading buffer 4× (125 mM Tris-HCl pH 6.8, 6% SDS, 4 M urea, 4 mM EDTA, 30% glycerol, 4% 2-mercaptoethanol, and bromophenol blue). For Western blot, samples were denatured at 95°C and loaded on a 10% SDS-PAGE gel. Separated proteins were transferred onto a nitrocellulose membrane (Biorad Turbo Nitrocellulose, catalog 1704158) by means of the Trans-blot Turbo Transfer System (Bio-Rad) (protocol: 1.5 A constant; up to 25 V; 20 minutes). Membranes were blocked with 5% nonfat milk in TBST for 1 hour and were then incubated overnight at 4°C with rabbit monoclonal anti-HA (1:1000; Cell Signalling, catalog C29F4), anti-FLAG (1:1000; Invitrogen, Thermo Fisher Scientific, catalog MA1-91878), and mouse monoclonal anti α-Tubulin (1:5000; MilliporeSigma, catalog T9026) antibodies in TBST. After washing, filters were incubated for 1 hour at room temperature with secondary antibodies (1:3000; Bio-Rad, goat anti-rabbit HRP, catalog 1706515, goat anti-mouse HRP, catalog 1706516) prepared in 5% milk in TBST. The Clarity Western ECL Substrate (Bio-Rad, catalog 1705061) was used to visualize immunoreactive bands. Blot visualization was performed by using the ChemiDoc MP Imaging System (Bio-Rad).

RNA preparation and retrotranscription. Total RNA was isolated from 200–300 mg of mouse tissue using 2 ml TRIzol reagent (Invitrogen, Thermo Fisher Scientific, catalog 15596026) after the tissues had been homogenized in liquid nitrogen with a mortar and pestle. To enhance RNA yield, the samples were precipitated by adding 2 μl glycogen solution (10 mg/ml) to isopropanol and incubating them at –80°C overnight. The concentration of RNA was evaluated spectrophotometrically, and its quality was verified by means of agarose gel electrophoresis of 1 μg of each sample. Genomic DNA was digested using 1 U rDNaseI (Invitrogen, Thermo Fisher Scientific, catalog AM1906) per 1 μg/μl of total RNA and incubated at 37°C for 10 minutes following the manufacturer's instructions. The total RNA was stored in aliquots at –80°C. Total RNA (1 μg) was reverse transcribed to single-stranded cDNA using Superscript III RNaseH reverse transcriptase (Invitrogen, Thermo Fisher Scientific, catalog 18080-044) and random primers (Invitrogen, Thermo Fisher Scientific, catalog 48190-011) in a volume of 20 μl, according to the manufacturer's instructions.

Real-time PCR. We used an iCycler Thermal Cycler with a Multicolour Real-time PCR Detection System (Bio-Rad). All reactions were performed in a total volume of 25 µl with 5 µl of cDNA, 20 µl iQTM SYBR Green Supermix (Bio-Rad, catalog 17088 80), and 0.2 µM each of forward and reverse primers. The amplification consisted of the following: 95°C for 3 minutes, 45 cycles of 30 seconds at 95°C, 30 seconds at 60°C, and 30 seconds at 72°C. Fluorescence was quantified during the annealing step, and product formation was confirmed by melting curve analysis (55°C–94°C). The following primers were used: ADAM10 forward: GGAAGCTTTAGTCATGGGTCTG; ADAM10 reverse: CTCCTTCCTCTACTCCAGTCAT; β-actin forward: AGTGTGACGTTGACATCCGTA; β-actin reverse: GCCAGAGCAGTAATCTCCTTCT; h18S forward: CGGCTACCACATCCAAGGAA; h18S reverse: GCTGGAATTACCGCGGCT; and hHTT forward: CGCTATGGAACTTTTTCTGCTGTG; hHTT reverse: CTGTAACCTTGGAAGATTAGAATCCATC. Data were analyzed by using the software Bio-Rad CFX Manager V.1.6.541.1028.

Brain slice preparation for biochemistry and electrophysiology. Acute brain slices were prepared from 11- to 12-week-old WT and R6/2 mice and from 54-week-old WT and zQ175 mice. For biochemical experiments, mice were anesthetized by i.p. injection of 10 mg/ml avertine and perfused in PBS 1×. After brain dissection, 300 µm thick coronal slices were cut on a Vibratome (Leica, catalog VT1000S) in cold PBS solution supplemented with 15 mM glucose, placed on membrane inserts, and incubated in Petri dishes with aCSF containing 125 mM NaCl, 2.5 mM KCl, 25 mM NaHCO3, 1.25 mM NaH2PO4, 6 mM MgCl2, 2 mM CaCl2, and 10 mM glucose. Brain slices were incubated with GI254023X at concentrations of 1, 10, 100, and 1000 nM for 45 minutes at 37°C and total protein lysates were prepared for Western blot as previously described. For electrophysiology experiments, animals were anesthetized by inhalation of isoflurane and transcardially perfused with cold (<4°C), carboxygenated (95% O_2, 5% CO_2) cutting solution (70 mM sucrose, 80 mM NaCl, 2.5 mM KCl, 26 mM NaHCO3, 15 mM glucose, 7 mM MgCl2, 1 mM CaCl2, 1.25 mM NaH2PO4). Coronal 300 µm thick slices were transferred to an incubation chamber filled with carboxygenated aCSF medium (125 mM NaCl, 2.5 mM KCl, 26 mM NaHCO3, 15 mM glucose, 1.3 mM MgCl2, 2.3 mM CaCl2, 1.25 mM NaH2PO4). For electrophysiological studies, GI254023X was used at concentrations of 50 nM for 45 minutes. All recordings were performed at 23–25°C on submerged slices perfused at 0.6 ml/minutes with aCSF. The recording chamber was mounted on an E600FN microscope equipped with a 4× lens and a 40× water-immersion objective (Nikon) and connected to a near-infrared CCD camera. The data were derived from striatal MSNs using the whole-cell patch-clamp technique in voltage- and current-clamp mode. Pipettes were produced from borosilicate glass capillary tubes (Hilgenberg GmbH) by means of a horizontal puller (P-97, Sutter Instruments) and filled with the following intracellular solution: 130 mM K-gluconate, 4 mM NaCl, 2 mM MgCl2, 1 mM EGTA, 5 mM creatine phosphate, 2 mM Na2ATP, 0.3 mM Na3GTP, and 10 mM HEPES (pH 7.3 with KOH). Membrane voltage was corrected off-line for a measured liquid junction potential. Series resistance was always compensated by 70%–90% and monitored throughout the experiment. Recordings were made with a MultiClamp 700B amplifier (Molecular Devices) and digitized with a Digidata 1322 computer interface (Molecular Devices). Data were acquired using the software Clampex 9.2 (Molecular Device), sampled at 20 kHz, and filtered at 10 kHz. All drugs were added to the aCFS medium. The EPSC recordings were carried out at the holding potential of –70 mV and in the presence of 10 µM bicuculline (Sigma-Aldrich, catalog 14343). Miniature EPSCs (mEPSCs) were derived in the presence of 1 µM TTX (Sigma-Aldrich, catalog T8024). To test the effect of 50 nM GI254023X, slices were incubated with the drug for 45 minutes before and during the recording. Data were analyzed with the software Clampfit 10.2 (Molecular Devices) and Origin (Microcal). Cell surface was estimated by integrating the capacitive current evoked by a −10 mV pulse. Neuronal R_{in} was calculated in the linear portion of the I-V relationship during depolarizing voltage responses near the V_m. The EPSCs were detected manually: the amplitude of the events obeyed a log-normal distribution and, accordingly, the mean amplitudes were computed using a log-normal function; the interevent intervals were distributed exponentially, and mean frequencies were obtained from the best monoexponential fit of each distribution.

Electron microscopy. Mice were anesthetized with 10 mg/ml avertin and transcardially perfused using 2.5% glutaraldehyde (Electron Microscopy Sciences, catalog 16220), and 2% paraformaldehyde (Electron Microscopy Sciences, catalog 19200) as fixatives, both in sodium cacodylate buffer 0.15 M (pH 7.4) (Electron Microscopy Sciences, catalog 12300). Brains were removed and post-fixed for an additional 24 hours at 4°C, and 100 µm thick coronal slices were cut by using a Leica VT1000S Vibratome. Sections were collected in 0.1 M sodium cacodylate buffer, and striatum was manually dissected for staining and embedding. Samples were then washed with 0.1 M cold sodium cacodylate buffer and then postfixed in a reduced osmium solution (i.e., 1.5% potassium ferrocyanide, Electron Microscopy Sciences, catalog 20150) with 2% osmium tetroxide (Electron Microscopy Sciences, catalog 19170) in 0.15 M cacodylate buffer for 1 hour on ice. After the first heavy metal incubation, the tissues were washed with ddH_2O at room temperature and then placed in the 0.22 µm Millipore-filtered 1% thiocarbohydrazide (TCH) (Electron Microscopy Sciences, catalog 21900) in ddH_2O solution for 20 minutes at room temperature. Tissues were then rinsed again in ddH_2O and incubated in 2% osmium tetroxide in ddH_2O for 30 minutes at room temperature. After several washings at room temperature in ddH_2O, they were then placed in 1% uranyl acetate (aqueous) and left overnight at 4°C. Samples were washed once again and then immersed en bloc in Walton's lead aspartate solution (0.066 gr lead nitrate, Electron Microscopy Sciences, catalog 17900) dissolved in 10 ml of 0.003 M aspartic acid solution, pH 5.5) at 60°C for 30 minutes. The tissues were washed and then dehydrated stepwise through an ethanol series and finally placed in anhydrous ice-cold acetone for 10 minutes. Infiltration was performed with an acetone (Sigma-Aldrich, catalog 179124)/Durcupan ACM (Electron Microscopy Sciences, catalog 14040) mixture with 3:1 volume proportions for 2 hours, then 1:1 overnight. The tissues were left for 2 hours in pure resin and then embedded in Durcupan ACM resin and placed in a 60°C oven for 48 hours for polymerization. For TEM imaging, ultrathin sections 70 nm thick were prepared by an UltraCut E Ultramicrotome (Reichert) and placed on TEM copper grids, which were then observed using a LEO 912AB microscope (Carl Zeiss) equipped with a thermionic W electron source and operating at an acceleration voltage of 100 kV. For quantitative analyses, images (resolution: 1024 × 1024 pixels) were acquired using a bottom mount Esivision CCD-BM/1K system (ProScan Camera). Quantitative measurements were performed by ImageJ, version 1.47 (NIH), and mea-

suring the following parameters: SVs number per area unit (μm^2), number of docked vesicles per active zone (AZ), AZ length (μm), and PSD length (nm). For SBF-SEM imaging, resin blocs were mounted on aluminium specimen pins and trimmed with a glass knife using an Ultramicrotome in order to expose the tissue on all 4 sides. Silver paint (TedPella, catalog 16031) was used to electrically ground the edges of the tissue block to the aluminium pin. The entire specimen was then sputter coated with a thin layer of gold in order to finely mount it into the SEM chamber in view of the SBF-SEM imaging. The blocks containing striatum were imaged using a Gatan 3View system (Gatan) attached to a FEI Quanta FEG 200 SEM equipped with a Schottky field emission electron source, operating at an accelerating voltage of 3 kV, and with a beam current of 21 pA, upon low-vacuum conditions (15 Pa). Serial SEM images were acquired collecting the backscattered electron (BSE) signal, with a magnification of ×10,000, a dwell time of 10 μs per pixel, and an image resolution of 2048 × 2048 pixels, corresponding to a final asymmetric voxel size of 6.7 × 6.7 × 50 nm^3. For 3D reconstruction, rendering, and analysis, serial SEM images were assembled into volume files aligned using Digital Micrograph (Gatan). For manual segmentation and 3D model generation, electron microscopy image stacks were then converted to 8-bit grayscale tiff format images and manually segmented using the AMIRA software package (FEI Company). 3D structures in image stacks containing hundreds or thousands of 2D orthoslices were traced individually in each plane and automatically surface rendered. The PSD volume was measured by the AMIRA 3D model using its Material Statistics module. The excitatory synapse density (n of excitatory synapse/μm^3) was measured by using Ilastik-0.5.12 software.

In vitro metalloprotease assay. The ADAM10 inhibitor GI254023X and ADAM17 inhibitor GW280264X were serially diluted in DMSO and transferred to a 384-well plate in a volume suitable to reach the desired compound concentrations in 20 μl of reaction buffer (TrisHCl 25 mM pH 9.0, 0.005% Brij-35, 2.5 μM $ZnCl_2$, 100 mM NaCl). ADAM10 (R&D Systems, catalog CF936-AD-020) was used at a final concentration of 2.5 nM, while ADAM17 (R&D Systems, catalog 930-ADB-010) was used at 1 nM. For both assays, the BML-P235-0001 substrate (Enzo Life Sciences) was used at 10 μM. The reaction was incubated at room temperature for 1 hour; then the cleaved substrate was revealed by florescence intensity according to the manufacturer's protocol.

Statistics. All measurements are presented as mean ± SEM. Prism 7.0c (GraphPad Software) was used to perform all statistical analyses. For each set of data to be compared, we determined in Prism whether data were normally distributed or not by using the D'Agostino-Pearson or Shapiro-Wilk normality test. For normally distributed values, statistical significance was determined by the unpaired Student's t test when 2 groups were compared while 1-way ANOVA followed by Newman-Keuls or Bonferroni's multiple comparison test was used when more than 2 groups were tested. For nonnormal distributed data, the nonparametric Mann-Whitney 2-tailed U test was used when 2 groups were compared,

while 1-way ANOVA followed by the nonparametric Dunn's multiple comparison test was used when more than 2 groups were tested. Differences were considered statistically significant at $P < 0.05$.

Study approval. All protocols involving animals were carried out in accordance with institutional guidelines in compliance with Italian law (D. Lgs no. 2014/26, implementation of the 2010/63/UE). The Ethics Committee of the University of Milano approved studies in mice (Ethics Committee 09.10.13, Ethical Approval 74/13; Ethics Committee 18.12.13, Ethical Approval 74/14) and the use of human postmortem samples obtained from HBTRC (Ethics Committee 18.12.13, Ethical Approval 74/14).

Author contributions

Acknowledgments

Address correspondence to: Chiara Zuccato, Department of Biosciences, University of Milan, Istituto Nazionale di Genetica Molecolare "Romeo ed Enrica Invernizzi," Via Sforza 35, 20122 Milano, Italy. Phone: 39.02.50325839; Email: chiara.zuccato@unimi.it.

1. [No authors listed]. A novel gene containing a trinucleotide repeat that is expanded unstable on Huntington's disease chromosomes. The Huntington's Disease Collaborative Research Group. *Cell*. 1993;72(6):971–983.
2. Rüb U, Seidel K, Heinsen H, Vonsattel JP, den Dunnen WF, Korf HW. Huntington's disease (HD): the neuropathology of a multisystem

neurodegenerative disorder of the human brain. *Brain Pathol*. 2016;26(6):726–740.
3. Shirasaki DI, et al. Network organization of the huntingtin proteomic interactome in mammalian brain. *Neuron*. 2012;75(1):41–57.
4. McKinstry SU, et al. Huntingtin is required for normal excitatory synapse development in cortical and striatal circuits. *J Neurosci*.

2014;34(28):9455–9472.
5. Cepeda C, Wu N, André VM, Cummings DM, Levine MS. The corticostriatal pathway in Huntington's disease. *Prog Neurobiol*. 2007;81(5-6):253–271.
6. Milnerwood AJ, Raymond LA. Early synaptic pathophysiology in neurodegeneration: insights from Huntington's disease. *Trends Neurosci*. 2010;33(11):513–523.

7. Ross CA, Pantelyat A, Kogan J, Brandt J. Determinants of functional disability in Huntington's disease: role of cognitive and motor dysfunction. *Mov Disord*. 2014;29(11):1351–1358.

8. Kuhn PH, et al. Systematic substrate identification indicates a central role for the metalloprotease ADAM10 in axon targeting and synapse function. *Elife*. 2016;5:12748.

9. Saftig P, Lichtenthaler SF. The alpha secretase ADAM10: A metalloprotease with multiple functions in the brain. *Prog Neurobiol*. 2015;135:1–20.

10. Prox J, et al. Postnatal disruption of the disintegrin/metalloproteinase ADAM10 in brain causes epileptic seizures, learning deficits, altered spine morphology, and defective synaptic functions. *J Neurosci*. 2013;33(32):12915–12928, 12928a.

11. Jorissen E, et al. The disintegrin/metalloproteinase ADAM10 is essential for the establishment of the brain cortex. *J Neurosci*. 2010;30(14):4833–4844.

12. Clement AB, et al. Effects of neuron-specific ADAM10 modulation in an in vivo model of acute excitotoxic stress. *Neuroscience*. 2008;152(2):459–468.

13. Prinzen C, Trümbach D, Wurst W, Endres K, Postina R, Fahrenholz F. Differential gene expression in ADAM10 and mutant ADAM10 transgenic mice. *BMC Genomics*. 2009;10:66.

14. Lo Sardo V, et al. An evolutionary recent neuroepithelial cell adhesion function of huntingtin implicates ADAM10-Ncadherin. *Nat Neurosci*. 2012;15(5):713–721.

15. Mangiarini L, et al. Exon 1 of the HD gene with an expanded CAG repeat is sufficient to cause a progressive neurological phenotype in transgenic mice. *Cell*. 1996;87(3):493–506.

16. Menalled LB, et al. Comprehensive behavioral and molecular characterization of a new knock-in mouse model of Huntington's disease: zQ175. *PLoS ONE*. 2012;7(12):e49838.

17. Bichelmeier U, et al. Nuclear localization of ataxin-3 is required for the manifestation of symptoms in SCA3: in vivo evidence. *J Neurosci*. 2007;27(28):7418–7428.

18. Friedman MJ, et al. Polyglutamine domain modulates the TBP-TFIIB interaction: implications for its normal function and neurodegeneration. *Nat Neurosci*. 2007;10(12):1519–1528.

19. Kelp A, et al. A novel transgenic rat model for spinocerebellar ataxia type 17 recapitulates neuropathological changes and supplies in vivo imaging biomarkers. *J Neurosci*. 2013;33(21):9068–9081.

20. Malinverno M, et al. Synaptic localization and activity of ADAM10 regulate excitatory synapses through N-cadherin cleavage. *J Neurosci*. 2010;30(48):16343–16355.

21. Restituito S, et al. Synaptic autoregulation by metalloproteases and γ-secretase. *J Neurosci*. 2011;31(34):12083–12093.

22. Andreyeva A, et al. C-terminal fragment of N-cadherin accelerates synapse destabilization by amyloid-β. *Brain*. 2012;135(Pt 7):2140–2154.

23. Conforti P, et al. Faulty neuronal determination and cell polarization are reverted by modulating HD early phenotypes. *Proc Natl Acad Sci U S A*. 2018;115(4):E762–E771.

24. Hoettecke N, Ludwig A, Foro S, Schmidt B. Improved synthesis of ADAM10 inhibitor GI254023X. *Neurodegener Dis*. 2010;7(4):232–238.

25. Cepeda C, et al. Transient and progressive electrophysiological alterations in the corticostriatal pathway in a mouse model of Huntington's disease. *J Neurosci*. 2003;23(3):961–969.

26. Heikkinen T, et al. Characterization of neurophysiological and behavioral changes, MRI brain volumetry and 1H MRS in zQ175 knock-in mouse model of Huntington's disease. *PLoS ONE*. 2012;7(12):e50717.

27. Marcello E, et al. Synapse-associated protein-97 mediates alpha-secretase ADAM10 trafficking and promotes its activity. *J Neurosci*. 2007;27(7):1682–1691.

28. Epis R, et al. Blocking ADAM10 synaptic trafficking generates a model of sporadic Alzheimer's disease. *Brain*. 2010;133(11):3323–3335.

29. Murmu RP, Li W, Holtmaat A, Li JY. Dendritic spine instability leads to progressive neocortical spine loss in a mouse model of Huntington's disease. *J Neurosci*. 2013;33(32):12997–13009.

30. Murmu RP, Li W, Szepesi Z, Li JY. Altered sensory experience exacerbates stable dendritic spine and synapse loss in a mouse model of Huntington's disease. *J Neurosci*. 2015;35(1):287–298.

31. Hartmann D, et al. The disintegrin/metalloprotease ADAM 10 is essential for Notch signalling but not for alpha-secretase activity in fibroblasts. *Hum Mol Genet*. 2002;11(21):2615–2624.

32. Sepers MD, Raymond LA. Mechanisms of synaptic dysfunction and excitotoxicity in Huntington's disease. *Drug Discov Today*. 2014;19(7):990–996.

33. Mattis VB, et al. HD iPSC-derived neural progenitors accumulate in culture and are susceptible to BDNF withdrawal due to glutamate toxicity. *Hum Mol Genet*. 2015;24(11):3257–3271.